



Research article

On the numerical discretization of a tumor progression model driven by competing migration mechanisms[†]

Yangyang Qiao, Qing Li and Steinar Evje*

Faculty of Science and Technology, University of Stavanger, Stavanger, NO 4068, Norway

[†] **This contribution is part of the Special Issue:** Advances in the analysis of chemotaxis systems

Guest Editor: Michael Winkler

Link: www.aimspress.com/mine/article/6067/special-articles

* **Correspondence:** Email: steinar.evje@uis.no.

Abstract: In this work we explore a recently proposed biphasic cell-fluid chemotaxis-Stokes model which is able to represent two competing cancer cell migration mechanisms reported from experimental studies. Both mechanisms depend on the fluid flow but in a completely different way. One mechanism depends on chemical signaling and leads to migration in the downstream direction. The other depends on mechanical signaling and triggers cancer cells to go upstream. The primary objective of this paper is to explore an alternative numerical discretization of this model by borrowing ideas from [Qiao et al. (2020), M3AS 30]. Numerical investigations give insight into which parameters that are critical for the ability to generate aggressive cancer cell behavior in terms of detachment of cancer cells from the primary tumor and creation of isolated groups of cancer cells close to the lymphatic vessels. The secondary objective is to propose a reduced model by exploiting the fact that the fluid velocity field is largely dictated by the draining fluid from the leaky tumor vasculature and collecting peritumoral lymphatics and is more weakly coupled to the cell phase. This suggests that the fluid flow equations to a certain extent might be decoupled from the cell phase equations. The resulting model, which represents a counterpart of the much studied chemotaxis-Stokes model proposed by [Tuval, et al. (2005), PNAS 102], is explored by numerical experiments in a one-dimensional tumor setting. We find that the model largely coincides with the original as assessed through numerical solutions computed by discrete schemes. This model might be more amenable for further explorations and analysis. We also investigate how to exploit the weaker coupling between cell phase dynamics and fluid dynamics to do more efficient calculations with fewer updates of the fluid pressure and velocity field.

Keywords: cell-migration; multiphase flow; interstitial fluid; chemotaxis; reduced model; lymphatic flow; vascular flow; metastasis

1. Introduction

1.1. Background

The phenomenon of lymph node metastasis has been recognized for a long time. However, the underlying mechanism by which malignant tumor cells leave the primary tumor site, invade the lymphatics and metastasize to lymph nodes are unclear [11]. In [12, 24] it is suggested that interstitial flow (IF) caused by lymphatic drainage directs tumor cell migration by utilizing interstitial flow to create and amplify gradients of a chemical agent (chemokine) and thus move by chemotaxis toward the lymphatic in a process termed autologous chemotaxis. Polacheck et al. [16] extended the study by Shields et al. [24], demonstrating that the strength of flow as well as the cell seeding density affected the migration direction. Their work provides further evidence that autologous chemotaxis is the mechanism that leads to cancer cell migration with the flow, but there is another mechanism that causes strain-induced migration against the flow. It was shown that a low cell seeding density culture migrated with the flow in accordance with the behavior reported in [24]. However, for a high cell seeding density the migration was dominated by upstream migration. In addition, this migration against the flow direction was sensitive to the fluid velocity. Higher fluid velocity increased the upstream migration. Moreover, when chemotaxis was blocked, both high and low density cultures migrated upstream. Polacheck et al. further investigated the effects of interstitial fluid flow stresses imparted on cells [17]. A first attempt to describe the phenomenon of autologous chemotaxis theoretically in a continuum setting where both cancer cells and fluid are represented through separate mass and momentum equations [2], can be found in [30]. The model was based on a biphasic cell-fluid-matrix formulation where matrix is assumed to be stagnant occupying a certain volume $1 - \phi$ of the bulk volume whereas cells and fluid compete for space in the remaining void volume described by the porosity ϕ . Various model parameters were determined to comply with the experimental results in [12, 24] regarding a realistic fluid velocity and cell migration velocity. In particular, efforts were made to explain the role of a governing component of the cell velocity reflecting chemotaxis-driven motion toward a chemical agent (chemokine) that is skewed in the flow direction. A step further was taken in [31] where the biphasic model was extended to account for the mechanically induced upwind migration component reported in [16]. (Further modeling of this phenomenon can be found in [23]). The resulting model was shown to capture many of the trends reported in [16] concerning the internal competition between the downstream chemotaxis migration and the fluid-stress related upstream migration. However, an open question is to what extent these competing mechanisms can play a role as a possible driver for metastatic behavior? That is, to what extent are tumor cells at the periphery of the primary tumor able to detach from the primary tumor, a behavior that might pave the way for lymph node metastasis where cancer cells escape to nearby lymphatic vessels? For further discussion and some preliminary investigations of that issue we refer the reader to [8].

1.2. Main objectives

The purpose of the current work is to take a closer look at different aspects of the biphasic cell-fluid model and try to put the model into a larger context. We start reviewing a slightly simplified version of the model studied in [8, 31] where the chemical agents that are involved have been reduced

from three to one. This is done while maintaining the same competing migration mechanisms. The first question we are interested in is: How can we make use of a general and robust discretization method to obtain numerical reliable approximations of the true solution? The idea we employ is to borrow techniques from a recent study of a cell-fluid model, which represents a biphasic description of the model introduced in the seminal work [29] of cell swimming, that was explored in [19]. Secondly, we use the novel discretization and explore in a one-dimensional tumor setting to what extent the model possesses a detachment mechanism, as explained above. The third question we pay attention to is: Can we derive a version of the cell-fluid-matrix model that resembles the Tuval model presented in [29]? This is partly motivated by the fact that this model appears to be ideal for systematical studies of the interplay between fluid dynamics, as described by the incompressible (Navier-)Stokes formulation, and chemotactic-driven cell motion. The model has released a rather intense study of finer details, as revealed through mathematical analysis, involved in the competing forces that ultimately dictate the cell-fluid dynamics [1, 3, 6, 13, 27, 28, 33]. The fourth question is a natural consequence of this last model: How can we exploit the fact that the fluid dynamics apparently depend weakly on the explicit presence of cancer cells, whereas cancer cells are more sensitive to the fluid behavior?

2. A cell-fluid-matrix model

2.1. General multiphase formulation

In the multiphase modeling framework, the tumor-host environment is considered as a mixture of three interacting continua [2, 5, 9, 22]: the stagnant matrix, whose main component is extracellular matrix (ECM), that is described by a volume fraction $1 - \phi$; the cellular phase comprises tumor cells represented by a volume fraction α_c and density ρ_c moving within the pore space represented by porosity ϕ with an interstitial velocity \mathbf{u}_c^p ; and the extracellular fluid phase represented by the volume fraction α_w and density ρ_w moving with a velocity \mathbf{u}_w^p .

The resulting model is summed up below, and we refer to [7, 30, 31] for more details:

$$\begin{aligned}
 (\alpha_c \phi \rho_c)_t + \nabla \cdot (\alpha_c \phi \rho_c \mathbf{u}_c^p) &= 0 \\
 (\alpha_w \phi \rho_w)_t + \nabla \cdot (\alpha_w \phi \rho_w \mathbf{u}_w^p) &= \rho_w Q, & Q &= Q_v - Q_l \\
 \alpha_c \nabla P_c &= -\hat{\zeta}_c \mathbf{u}_c^p + \hat{\zeta}(\mathbf{u}_w^p - \mathbf{u}_c^p) + \varepsilon_c \nabla \cdot (\alpha_c \rho_c \nabla \mathbf{u}_c^p) \\
 \alpha_w \nabla P_w &= -\hat{\zeta}_w \mathbf{u}_w^p - \hat{\zeta}(\mathbf{u}_w^p - \mathbf{u}_c^p) + \varepsilon_w \nabla \cdot (\alpha_w \rho_w \nabla \mathbf{u}_w^p) \\
 (\alpha_w \phi C)_t + \nabla \cdot (\alpha_w \phi C \mathbf{u}_w^p) &= \nabla \cdot (D_C \nabla C) + R_C, & \mathbf{x} \in \Omega
 \end{aligned} \tag{2.1}$$

with additional algebraic equations and correlations given by

$$\begin{aligned}
 \alpha_c + \alpha_w &= 1 \\
 P_c &= P_w + \Delta P(\alpha_c) + \Lambda(C) \\
 R_C &= \alpha_c(1 - \alpha_c)\lambda_1 \left(1 - \left(\frac{C}{C_M}\right)^{\nu_c}\right) - C(\lambda_2 \alpha_c + \lambda_3 Q_l) \\
 Q_v &= T_v(\mathbf{x})(\tilde{P}_v^* - P_w) & Q_l &= T_l(\mathbf{x})(P_w - \tilde{P}_l^*)
 \end{aligned} \tag{2.2}$$

The first two equations of (2.1) describe the mass balance for cancer cells and fluid, respectively, as they compete for the same pore space. Equation (2.2)₁ expresses that cells and fluid completely occupy the

pore space. The blood circulation associated with the leaky and aberrant tumor vasculature is expressed through $Q = Q_v - Q_l$ involved in (2.1)₂. Generally, we may consider the phases as compressible fluids by specifying appropriate pressure-density closure relations $\rho_i = \rho_i(P_i)$, $i = c, w$. The two subsequent equations (2.1)_{3,4} describe the corresponding momentum balance. In particular, the pressure gradient ∇P_c (cell phase) is balanced against the cell-matrix resistance force $-\hat{\zeta}_c \mathbf{u}_c^p$ whereas the interaction term $\hat{\zeta}(\mathbf{u}_w^p - \mathbf{u}_c^p)$ accounts for a force generated by the cancer cells in response to the stress from the flowing fluid. The last term describes internal viscous effects. Similarly, (2.1)₄ describes how the fluid pressure gradient ∇P_w is balanced by a fluid-matrix resistance force $-\hat{\zeta}_w \mathbf{u}_w^p$ followed by the cell-fluid interaction term and internal viscosity. In Section 4 we provide further information how the parameters involved in $\hat{\zeta}_w$, $\hat{\zeta}_c$, and $\hat{\zeta}$ in (2.1)_{3,4} are set. The last equation (2.1)₅ accounts for the chemical agent C which is secreted from the cancer cells and move by diffusion and fluid velocity \mathbf{u}_w^p .

The cell phase pressure P_c feels additional stress due to cell-cell interaction through $\Delta P(\alpha_c)$ and migration-related stress due to chemotaxis through $\Lambda(C)$, as expressed by the relation (2.2)₂. Similar to [7, 30, 31], we use

$$\Delta P(\alpha_c) = -\gamma \ln(1 - \alpha_c) \quad (2.3)$$

and

$$\Lambda(C) = -\Lambda_1 \frac{C}{C_M} \quad (2.4)$$

where C_M represents a maximal concentration. The reaction term R_C in (2.2)₃ accounts for production of chemokine by the cancer cells themselves (the first bracket) and consumption and absorption through the lymphatic drainage (second bracket). The last line (2.2)₄ describes that the fluid produced by the blood vasculature in the tumor through Q_v is controlled by the internal vascular pressure \tilde{P}_v^* and the conductivity associated with the blood vessel wall through T_v . Similarly for the lymphatic absorption of fluid through Q_l . We refer to Section 4 for more information how parameters are set, including (2.3) and (2.4).

Assuming a constant porosity ϕ where we rescale the time variable $t \rightarrow t/\phi$ and introduce a phase velocity $\mathbf{u}_c = \phi \mathbf{u}_c^p$ and $\mathbf{u}_w = \phi \mathbf{u}_w^p$, we may write the model in the form

$$\begin{aligned} (\alpha_c \rho_c)_t + \nabla \cdot (\alpha_c \rho_c \mathbf{u}_c) &= 0 \\ (\alpha_w \rho_w)_t + \nabla \cdot (\alpha_w \rho_w \mathbf{u}_w) &= \rho_w Q, \quad Q = Q_v - Q_l \\ \alpha_c \nabla P_c &= -\hat{\zeta}_c \mathbf{u}_c + \hat{\zeta}(\mathbf{u}_w - \mathbf{u}_c) + \varepsilon_c \nabla \cdot (\alpha_c \rho_c \nabla \mathbf{u}_c) \\ \alpha_w \nabla P_w &= -\hat{\zeta}_w \mathbf{u}_w - \hat{\zeta}(\mathbf{u}_w - \mathbf{u}_c) + \varepsilon_w \nabla \cdot (\alpha_w \rho_w \nabla \mathbf{u}_w) \\ (C)_t + \nabla \cdot (C \mathbf{u}_w) &= \nabla \cdot (D_C \nabla C) + R_C, \quad \mathbf{x} \in \Omega. \end{aligned} \quad (2.5)$$

Here we have also implicitly absorbed ϕ in the coefficients $\hat{\zeta}_c$, $\hat{\zeta}_w$, $\hat{\zeta}$, and ε_c , ε_w . We have also used the approximation $C \alpha_w \approx C$ for the transport equation describing C .

2.2. Incompressible and inviscid version

Following [30] we assume fluids are incompressible. This allows us to derive an explicit expression for the interstitial cell velocity \mathbf{u}_c which reflects the competition between different migration mechanisms as well the role played by the different interaction terms $\hat{\zeta}_w$, $\hat{\zeta}_c$, and $\hat{\zeta}$. From

(2.1) we obtain the following dimensionless simplified version:

$$\begin{aligned}
\alpha_{ct} + \nabla \cdot (\alpha_c \mathbf{u}_c) &= 0 \\
\alpha_{wt} + \nabla \cdot (\alpha_w \mathbf{u}_w) &= Q_v - Q_l \\
\alpha_c \nabla (P_w + \Delta P + \Lambda(C)) &= -\hat{\zeta}_c \mathbf{u}_c + \hat{\zeta}(\mathbf{u}_w - \mathbf{u}_c) + \varepsilon_c \rho_c \nabla \cdot (\alpha_c \nabla \mathbf{u}_c) \\
\alpha_w \nabla P_w &= -\hat{\zeta}_w \mathbf{u}_w - \hat{\zeta}(\mathbf{u}_w - \mathbf{u}_c) + \varepsilon_w \rho_w \nabla \cdot (\alpha_w \nabla \mathbf{u}_w) \\
C_t + \nabla \cdot (C \mathbf{u}_w) &= \nabla \cdot (D_C \nabla C) + R_C, \quad \mathbf{x} \in \Omega.
\end{aligned} \tag{2.6}$$

The model is combined with the boundary conditions

$$P_w \Big|_{\partial\Omega} = P^*, \quad \frac{\partial}{\partial \nu} C \Big|_{\partial\Omega} = 0, \quad t > 0 \tag{2.7}$$

where ν is the outward normal on $\partial\Omega$ and P^* a known pressure at the boundary. Corresponding initial data are

$$\alpha_c(\mathbf{x}, t = 0) = \alpha_{c0}(\mathbf{x}), \quad C(\mathbf{x}, t = 0) = C_0(\mathbf{x}). \tag{2.8}$$

From the two momentum equations (2.6)_{3,4} we can compute explicit expressions for the cell and fluid velocity, respectively, \mathbf{u}_c and \mathbf{u}_w , by ignoring the viscous terms, i.e., we set $\varepsilon_c = \varepsilon_w = 0$. We refer to [30] for details. The following expressions are found:

$$\begin{aligned}
\mathbf{u}_c &= \mathbf{U}_T \left[\frac{\hat{f}_c(\alpha_c)}{\alpha_c} \right] - \left[\frac{\hat{h}(\alpha_c)}{\alpha_c} \right] \nabla (\Delta P + \Lambda), \\
\mathbf{u}_w &= \mathbf{U}_T \left[\frac{\hat{f}_w(\alpha_c)}{\alpha_w} \right] + \left[\frac{\hat{h}(\alpha_c)}{\alpha_w} \right] \nabla (\Delta P + \Lambda),
\end{aligned} \tag{2.9}$$

where $\mathbf{U}_T = \alpha_w \mathbf{u}_w + \alpha_c \mathbf{u}_c$ and with fractional flow functions $\hat{f}_c(\alpha_c)$ and $\hat{f}_w(\alpha_c)$ given by

$$\begin{aligned}
\hat{f}_c(\alpha_c) &:= \frac{\hat{\lambda}_c}{\hat{\lambda}_T} = \frac{[\alpha_c^2 \hat{\zeta}_w] + \alpha_c \hat{\zeta}}{[\alpha_c^2 \hat{\zeta}_w] + [\alpha_w^2 \hat{\zeta}_c] + \hat{\zeta}}, \\
\hat{f}_w(\alpha_c) &:= \frac{\hat{\lambda}_w}{\hat{\lambda}_T} = \frac{[\alpha_w^2 \hat{\zeta}_c] + \alpha_w \hat{\zeta}}{[\alpha_c^2 \hat{\zeta}_w] + [\alpha_w^2 \hat{\zeta}_c] + \hat{\zeta}}, \\
\hat{h}(\alpha_c) &= \frac{\alpha_c^2 \alpha_w^2}{\alpha_c^2 \hat{\zeta}_w + \alpha_w^2 \hat{\zeta}_c + \hat{\zeta}},
\end{aligned} \tag{2.10}$$

where the coefficients $\hat{\lambda}_c$, $\hat{\lambda}_w$, and $\hat{\lambda}_T$ (so-called mobility functions [37]) are given by

$$\hat{\lambda}_c = \frac{[\alpha_c^2 \hat{\zeta}_w] + \alpha_c \hat{\zeta}}{\hat{\zeta}_c \hat{\zeta}_w + \hat{\zeta}[\hat{\zeta}_c + \hat{\zeta}_w]}, \quad \hat{\lambda}_w = \frac{[\alpha_w^2 \hat{\zeta}_c] + \alpha_w \hat{\zeta}}{\hat{\zeta}_c \hat{\zeta}_w + \hat{\zeta}[\hat{\zeta}_c + \hat{\zeta}_w]}, \tag{2.11}$$

and total mobility $\hat{\lambda}_T$ given by

$$\hat{\lambda}_T = \hat{\lambda}_c + \hat{\lambda}_w = \frac{[\alpha_c^2 \hat{\zeta}_w] + [\alpha_w^2 \hat{\zeta}_c] + \hat{\zeta}}{\hat{\zeta}_c \hat{\zeta}_w + \hat{\zeta}[\hat{\zeta}_c + \hat{\zeta}_w]}. \tag{2.12}$$

The model (2.6) then takes the more compact form:

$$\begin{aligned}\alpha_{ct} + \nabla \cdot (\alpha_c \mathbf{u}_c) &= 0 \\ C_t + \nabla \cdot (C \mathbf{u}_w) &= \nabla \cdot (D_C \nabla C) + R_C, \quad \mathbf{x} \in \Omega\end{aligned}\quad (2.13)$$

where \mathbf{u}_c is given by (2.9)₁. Note that we also need \mathbf{u}_w given by (2.9)₂ to solve (2.13)₂. Moreover, in order to compute \mathbf{U}_T we first solve the elliptic problem for P_w (see [30] for details)

$$-(Q_v - Q_l) - \nabla \cdot (\hat{\lambda}_c \nabla (\Delta P + \Lambda)) = \nabla \cdot (\hat{\lambda}_T \nabla P_w), \quad P_w \Big|_{\partial\Omega} = P^*. \quad (2.14)$$

Knowing P_w , we can compute \mathbf{U}_T needed in (2.9). We have the following expression for \mathbf{U}_T [30]:

$$\mathbf{U}_T = -\hat{\lambda}_T \nabla P_w - \hat{\lambda}_c \nabla (\Delta P + \Lambda). \quad (2.15)$$

Previous discretization [30, 31] has been based on the formulation (2.13)–(2.15) combined with the expressions (2.9)–(2.12). In the following, we describe another approach which is based on the original formulation (2.6) and which is motivated by more recent investigations of incompressible and compressible multiphase flow models for creeping fluids in a porous media [18, 20, 21, 25]. These models do not involve any chemotaxis transport mechanisms. The approach we explore in the current work builds on the discretization of a cell-fluid model presented in [19]. However, that model is nevertheless different from the tumor model we study here since it only involves a downstream chemotactic migration and not the mechanical upstream migration mechanism. The main advantage of this approach is that it can naturally deal with the more general case where both viscous terms (internal viscosity) are included as well as compressible fluids. In the following, for the sake of simplicity, we assume incompressibility.

2.3. A general discretization method based on the original full model (2.6)

The dimensionless domain $\Omega = [0, 1]$ is considered for the one-dimensional model. We introduce the approximate cell volume fraction and chemokine concentration $\{\alpha_{cj}(t)\}_{j=1}^N$ and $\{C_j(t)\}_{j=1}^N$ and fluid pressure $\{P_{wj}(t)\}_{j=1}^N$ associated with the nodes $\{x_j\}_{j=1}^N$ whereas the approximate velocities $\{u_{w,j+1/2}\}_{j=0}^N$ and $\{u_{c,j+1/2}\}_{j=0}^N$ are associated with the grid block interfaces $\{x_{j+1/2}\}_{j=0}^N$. That is, grid block center positions are given by

$$x_1 = \frac{1}{2}\Delta x, \quad x_2 = (1 + \frac{1}{2})\Delta x, \quad \dots, \quad x_j = (j - \frac{1}{2})\Delta x, \quad \dots, \quad x_{N_x} = (N - \frac{1}{2})\Delta x$$

and corresponding grid block interfaces $x_{j+1/2}$ are given by

$$x_{1/2} = 0, \quad x_{3/2} = \Delta x, \quad \dots, \quad x_{j+1/2} = j\Delta x, \quad \dots, \quad x_{N+1/2} = N\Delta x = 1,$$

where $\Delta x = 1/N$.

We assume that we have an approximate solution $(\alpha_{c,j}^k, C_j^k, P_{w,j}^k, u_{c,j+1/2}^k, u_{w,j+1/2}^k)$ at time t^k . Next, we describe how to obtain a new approximate solution $(\alpha_{c,j}^{k+1}, C_j^{k+1}, P_{w,j}^{k+1}, u_{c,j+1/2}^{k+1}, u_{w,j+1/2}^{k+1})$ at time t^{k+1} through a 2-step algorithm.

Step 1: Mass transport

We solve for $(\alpha_{c,j}^{k+1}, C_j^{k+1})$ by using the following discrete version of (2.6)₁ and (2.6)₅, respectively:

$$\frac{\alpha_{c,j}^{k+1} - \alpha_{c,j}^k}{\Delta t} + \frac{1}{\Delta x}([\alpha_c u_c]_{j+1/2}^k - [\alpha_c u_c]_{j-1/2}^k) = 0 \quad (2.16)$$

where

$$[\alpha_c u_c]_{j+1/2}^k = \begin{cases} \alpha_{c,j}^k u_{c,j+1/2}^k, & \text{if } u_{c,j+1/2}^k \geq 0; \\ \alpha_{c,j+1}^k u_{c,j+1/2}^k, & \text{if } u_{c,j+1/2}^k < 0. \end{cases} \quad (2.17)$$

$$\frac{C_j^{k+1} - C_j^k}{\Delta t} + \frac{1}{\Delta x}([Cu_w]_{j+1/2}^k - [Cu_w]_{j-1/2}^k) = \frac{D_c}{\Delta x} \left[\frac{C_{j+1}^k - C_j^k}{\Delta x} - \frac{C_j^k - C_{j-1}^k}{\Delta x} \right] + R_{C,j}^k \quad (2.18)$$

where

$$[Cu_w]_{j+1/2}^k = \begin{cases} C_j^k u_{w,j+1/2}^k, & \text{if } u_{w,j+1/2}^k \geq 0; \\ C_{j+1}^k u_{w,j+1/2}^k, & \text{if } u_{w,j+1/2}^k < 0. \end{cases} \quad (2.19)$$

and

$$R_{C,j}^k = \lambda_1 \alpha_{c,j}^k (1 - \alpha_{c,j}^k) \left(1 - \left(\frac{C_j^k}{C_M}\right)^{\nu_2}\right) - (\lambda_2 \alpha_{c,j}^k + \lambda_3 T_{l,j}(P_{w,j}^k - \tilde{P}_l^*)) C_j^k \quad (2.20)$$

Then, we compute $\alpha_{w,j}^{k+1}$ from (2.2)₁. Next, we compute pressure and velocities simultaneously at time level $k + 1$.

Step 2: Computation of velocities and pressure

We solve for $P_{w,j}^{k+1}$, $u_{c,j+1/2}^{k+1}$ and $u_{w,j+1/2}^{k+1}$ by considering the following algebraic system, which is a discrete version of the sum of (2.6)₁ and (2.6)₂, combined with (2.6)_{3,4}:

$$\begin{aligned} \frac{1}{\Delta x}([\alpha_c^{k+1} u_c^{k+1}]_{j+1/2} - [\alpha_c^{k+1} u_c^{k+1}]_{j-1/2}) + \frac{1}{\Delta x}([\alpha_w^{k+1} u_w^{k+1}]_{j+1/2} - [\alpha_w^{k+1} u_w^{k+1}]_{j-1/2}) \\ = Q_j^{k+1} = T_{v,j}(\tilde{P}_v^* - P_{w,j}^{k+1}) - T_{l,j}(P_{w,j}^{k+1} - \tilde{P}_l^*) \end{aligned} \quad (2.21)$$

which is combined with the momentum balance equations

$$\begin{aligned} \alpha_{w,j+1/2}^{k+1} \frac{1}{\Delta x} (P_{w,j+1}^{k+1} - P_{w,j}^{k+1}) &= -\hat{\zeta}_{w,j+1/2}^{k+1} u_{w,j+1/2}^{k+1} - \hat{\zeta}_{j+1/2}^{k+1} (u_{w,j+1/2}^{k+1} - u_{c,j+1/2}^{k+1}) \\ &+ \varepsilon_w \frac{\rho_w}{\Delta x^2} (\alpha_{w,j+1}^{k+1} [u_{w,j+3/2}^{k+1} - u_{w,j+1/2}^{k+1}] - \alpha_{w,j}^{k+1} [u_{w,j+1/2}^{k+1} - u_{w,j-1/2}^{k+1}]), \\ \alpha_{c,j+1/2}^{k+1} \frac{1}{\Delta x} (P_{w,j+1}^{k+1} - P_{w,j}^{k+1}) &= -\alpha_{c,j+1/2}^{k+1} \frac{1}{\Delta x} (\Delta P_{j+1}^{k+1} - \Delta P_j^{k+1} + \Lambda_{j+1}^{k+1} - \Lambda_j^{k+1}) \\ &- \hat{\zeta}_{c,j+1/2}^{k+1} u_{c,j+1/2}^{k+1} + \hat{\zeta}_{j+1/2}^{k+1} (u_{w,j+1/2}^{k+1} - u_{c,j+1/2}^{k+1}) \\ &+ \varepsilon_c \frac{\rho_c}{\Delta x^2} (\alpha_{c,j+1}^{k+1} [u_{c,j+3/2}^{k+1} - u_{c,j+1/2}^{k+1}] - \alpha_{c,j}^{k+1} [u_{c,j+1/2}^{k+1} - u_{c,j-1/2}^{k+1}]). \end{aligned} \quad (2.22)$$

For the cell-fluid interaction term $\hat{\zeta}(\alpha_c)$ we discretize as follows:

$$[\hat{\zeta}]_{j+1/2}^{k+1} = \begin{cases} \hat{\zeta}_j^{k+1}, & \text{if } u_{c,j+1/2}^k - u_{w,j+1/2}^k > 0; \\ \frac{\hat{\zeta}_j^{k+1} + \hat{\zeta}_{j+1}^{k+1}}{2}, & \text{if } u_{c,j+1/2}^k - u_{w,j+1/2}^k = 0; \\ \hat{\zeta}_{j+1}^{k+1}, & \text{if } u_{c,j+1/2}^k - u_{w,j+1/2}^k < 0. \end{cases} \quad (2.23)$$

For cell volume fraction α_c at interface $j + 1/2$ we use

$$[\alpha_c]_{j+1/2}^{k+1} = \begin{cases} \alpha_{c,j}^{k+1}, & \text{if } u_{c,j+1/2}^k - u_{w,j+1/2}^k > 0; \\ \frac{\alpha_{c,j+1}^{k+1} + \alpha_{c,j}^{k+1}}{2}, & \text{if } u_{c,j+1/2}^k - u_{w,j+1/2}^k = 0; \\ \alpha_{c,j+1}^{k+1}, & \text{if } u_{c,j+1/2}^k - u_{w,j+1/2}^k < 0. \end{cases} \quad (2.24)$$

For water volume fraction α_w interface $j + 1/2$ we use

$$[\alpha_w]_{j+1/2}^{k+1} = \begin{cases} \alpha_{w,j}^{k+1}, & \text{if } u_{w,j+1/2}^k - u_{c,j+1/2}^k > 0; \\ \frac{\alpha_{w,j+1}^{k+1} + \alpha_{w,j}^{k+1}}{2}, & \text{if } u_{w,j+1/2}^k - u_{c,j+1/2}^k = 0; \\ \alpha_{w,j+1}^{k+1}, & \text{if } u_{w,j+1/2}^k - u_{c,j+1/2}^k < 0. \end{cases} \quad (2.25)$$

These terms appear in product with the pressure gradients appearing on the left-hand-side of (2.22). The discretization of $[\hat{\zeta}_c^{k+1}]_{j+1/2}$ and $[\hat{\zeta}_w^{k+1}]_{j+1/2}$ appearing in (2.22) on the right-hand-side is based on upwind similar to the treatment of the terms $[\alpha_c]_{j+1/2}^{k+1}$ (2.24) and $[\alpha_w]_{j+1/2}^{k+1}$ (2.25), respectively.

3. A reduced cell-fluid-matrix model

Now, we want to derive a reduced version of the model (2.6). The key element is that we seek a model where we have decoupled to some extent the fluid dynamics from the cancer cell dynamics. More precisely, we seek to take advantage of the fact that fluid velocity field largely is dictated by the fluid-matrix resistance force $-\hat{\zeta}_w \mathbf{u}_w$ in (2.6)₄ and the leaky vasculature and collecting lymphatic vessels through $Q = Q_v - Q_l$ in (2.6)₂. Cancer cells, on the other hand, apparently are more sensitive to the fluid. The resulting model may be considered as a counterpart of the Tuval's model that have been used for cell-fluid dynamics [29] but now in a porous media setting where interaction with the stagnant matrix also is involved.

3.1. An incompressible version

We seek to take advantage of the fact that while the cancer cells are quite sensitive to the fluid flow, both through the downstream chemotaxis migration as well as the upstream fluid-stress driven migration, the interstitial fluid depends weakly on the presence of cancer cells. We may assume incompressible phases and consider an approximation and modification of (2.6) motivated by the rewritten form (2.13). The rationale behind the approximation is the following three points:

- (i) Fluid velocity typically is a 100-fold larger than cell migration velocity [16, 24]. This suggests that $\mathbf{U}_T \approx \alpha_w \mathbf{u}_w$.
- (ii) We want to ensure that the basic relation (2.15), which determines the fluid velocity field through a Darcy-like equation, is taken into account.

(iii) Experimental work has revealed that interstitial flow may cause shear stress ranging from pulsatile and turbulent (near vasculature network) to primarily laminar convection, with fluid velocity influenced by interstitial porosity and pressure as well as vasculature density, permeability (conductivity), and viscoelastic properties [4, 11]. This suggests that we use a full momentum equation for the fluid with inclusion of acceleration terms.

Taking these aspects into account, we suggest a cell-fluid-matrix model of the form

$$\begin{cases} (\alpha_c)_t + \nabla \cdot (\alpha_w \mathbf{u} \tilde{f}_c(\alpha_c)) = \nabla \cdot (\tilde{h}(\alpha_c) \Delta P'(\alpha_c) \nabla \alpha_c) + \nabla \cdot (\tilde{h}(\alpha_c) \Lambda'(C) \nabla C), \\ \rho(\mathbf{u}_t + (\mathbf{u} \cdot \nabla) \mathbf{u}) + \nabla P_w = -\frac{\alpha_w}{\lambda_T} \mathbf{u} - \frac{\tilde{\lambda}_c}{\lambda_T} \nabla(\Delta P(\alpha_c) + \Lambda(C)) + \eta \Delta \mathbf{u}, & \nabla \cdot (\alpha_w \mathbf{u}) = Q = Q_v - Q_l \\ C_t + \nabla \cdot (C \mathbf{u}) = \nabla \cdot (D_C \nabla C) + R_C. \end{cases} \quad (3.1)$$

Here $\mathbf{u} = \mathbf{u}_w$ and ρ refers to the fluid density (constant). In (3.1) we see the appearance of functions \tilde{f}_c , \tilde{f}_w , and \tilde{h} instead of \hat{f}_c , \hat{f}_w , and \hat{h} given by (2.10) signalling that there is a slight difference. Similarly for $\tilde{\lambda}_c$ and $\tilde{\lambda}_T$. This is explained in the next subsection. A more precise justification of using (3.1) to represent the biphasic model (2.6) is provided through the numerical experiments presented in Section 4. We may rewrite (3.1) in the form (essentially using $\nabla \cdot (\alpha_w \mathbf{u}) = Q$)

$$\begin{cases} (\alpha_c)_t + \alpha_w \mathbf{u} \cdot \nabla(\tilde{f}_c(\alpha_c)) = \nabla \cdot (\tilde{h}(\alpha_c) \Delta P'(\alpha_c) \nabla \alpha_c) + \nabla \cdot (\tilde{h}(\alpha_c) \Lambda'(C) \nabla C) - Q \tilde{f}_c(\alpha_c), \\ \rho(\mathbf{u}_t + (\mathbf{u} \cdot \nabla) \mathbf{u}) + \nabla P_w = -\frac{\alpha_w}{\lambda_T} \mathbf{u} - \frac{\tilde{\lambda}_c}{\lambda_T} \nabla(\Delta P(\alpha_c) + \Lambda(C)) + \eta \Delta \mathbf{u}, & \nabla \cdot (\alpha_w \mathbf{u}) = Q = Q_v - Q_l \\ C_t + \mathbf{u} \cdot \nabla C = \nabla \cdot (D_C \nabla C) + R_C - QC. \end{cases} \quad (3.2)$$

This model bears similarity to the chemotaxis-Navier-Stokes model [29] when $\alpha_w \approx 1$ and $Q = 0$. A typical variant of this model is given by

$$\begin{aligned} n_t + \mathbf{u} \cdot \nabla n &= D_n \Delta n - \nabla \cdot (n \nabla C) \\ \rho(\mathbf{u}_t + (\mathbf{u} \cdot \nabla) \mathbf{u}) + \nabla p &= n \nabla \Phi + \eta \Delta \mathbf{u}, & \nabla \cdot \mathbf{u} &= 0 \\ C_t + \mathbf{u} \cdot \nabla C &= D_C \Delta C + S(n, C). \end{aligned} \quad (3.3)$$

Here n is cell density, D_n cell diffusion coefficient, Φ gravitational potential, and $S(n, C)$ represents production/consumption of the chemical agent, possibly, under the influence of the cells n . Comparing (3.3)₂ and (3.1)₂, we see that the fluid field is affected by the cells through the buoyancy term $n \nabla \Phi$ in the first model, whereas the latter is under influence of the cell population through the resistance force term $-\frac{\alpha_w}{\lambda_T} \mathbf{u}$ on the right-hand-side and cell mobility-related term $\frac{\tilde{\lambda}_c}{\lambda_T} \nabla(\Delta P + \Lambda)$ of the momentum balance, as well as the equation $\nabla \cdot (\alpha_w \mathbf{u}) = Q$.

Remark 1. Numerical computations are carried out in Section 4 to explore features possessed by the reduced model (3.1). Some natural questions are: What is the difference between (3.1) and (2.6)? Can we ignore the term $\frac{\tilde{\lambda}_c}{\lambda_T} \nabla(\Delta P(\alpha_c) + \Lambda(C))$ in (3.1)₂? Can we replace $\alpha_w \mathbf{u}$ by \mathbf{u} appearing in (3.1)₁ and (3.1)₂ and through that provide a further decoupling of cell and fluid dynamics? Can we take advantage of the looser coupling between fluid phase and cell phase and improve the efficiency of computing numerical solutions by doing fewer calculations of the fluid velocity \mathbf{u}_w and pressure P_w ?

3.2. Derivation of the reduced model (3.1) from the biphasic model (2.6)

We want to build a numerical scheme for the reduced model (3.1) which makes use of the principles of the discrete scheme presented in Section 2.3 for the model (2.6). For that purpose we need to revisit calculations involved in Section 2.2 that give us expressions for the cell and fluid velocity \mathbf{u}_c and \mathbf{u}_w as well as the expressions for \hat{f}_c , \hat{f}_w , and \hat{h} . In particular, since the discretization of α_c and α_w given by (2.24) and (2.25) not necessarily obey (2.2)₁ at the interface $j + 1/2$, we should avoid using that.

From (2.6)_{3,4} we have the momentum balance when restricting ourselves to the one-dimensional setting (setting $\varepsilon_c = \varepsilon_w = 0$):

$$\begin{aligned}\alpha_c(P_w + \Delta P + \Lambda)_x &= -\hat{\zeta}_c u_c + \hat{\zeta}(u_w - u_c) \\ \alpha_w P_{wx} &= -\hat{\zeta}_w u_w - \hat{\zeta}(u_w - u_c).\end{aligned}\quad (3.4)$$

We solve for u_c and u_w from the two equations in (3.4) and find expressions of the form

$$\begin{aligned}u_c &= -\frac{(\alpha_c \hat{\zeta}_w + (\alpha_c + \alpha_w) \hat{\zeta}) P_{wx} + \alpha_c (\hat{\zeta}_w + \hat{\zeta}) (\Delta P + \Lambda)_x}{\hat{\zeta}_w \hat{\zeta}_c + \hat{\zeta} (\hat{\zeta}_w + \hat{\zeta}_c)} \\ u_w &= -\frac{(\alpha_w \hat{\zeta}_c + (\alpha_c + \alpha_w) \hat{\zeta}) P_{wx} + \alpha_c \hat{\zeta} (\Delta P + \Lambda)_x}{\hat{\zeta}_w \hat{\zeta}_c + \hat{\zeta} (\hat{\zeta}_w + \hat{\zeta}_c)}\end{aligned}\quad (3.5)$$

Having these two phase velocities, the total velocity $U_T = \alpha_c u_c + \alpha_w u_w$ can be obtained:

$$U_T (\approx \alpha_w u_w) = -\frac{[\alpha_c^2 \hat{\zeta}_w + \alpha_w^2 \hat{\zeta}_c + (\alpha_w + \alpha_c)^2 \hat{\zeta}] P_{wx} + [\alpha_c^2 (\hat{\zeta}_w + \hat{\zeta}) + \alpha_c \alpha_w \hat{\zeta}] (\Delta P + \Lambda)_x}{\hat{\zeta}_w \hat{\zeta}_c + \hat{\zeta} (\hat{\zeta}_w + \hat{\zeta}_c)}\quad (3.6)$$

Therefore, from (3.6)

$$\begin{aligned}P_{wx} &\approx -\frac{\alpha_w [\hat{\zeta}_w \hat{\zeta}_c + \hat{\zeta} (\hat{\zeta}_w + \hat{\zeta}_c)]}{\alpha_c^2 \hat{\zeta}_w + \alpha_w^2 \hat{\zeta}_c + (\alpha_c + \alpha_w)^2 \hat{\zeta}} u_w - \frac{\alpha_c^2 (\hat{\zeta}_w + \hat{\zeta}) + \alpha_w \alpha_c \hat{\zeta}}{\alpha_c^2 \hat{\zeta}_w + \alpha_w^2 \hat{\zeta}_c + (\alpha_c + \alpha_w)^2 \hat{\zeta}} (\Delta P + \Lambda)_x \\ &= -\frac{\alpha_w}{\tilde{\lambda}_T(\alpha_c, \alpha_w)} u_w - \frac{\tilde{\lambda}_c(\alpha_c, \alpha_w)}{\tilde{\lambda}_T(\alpha_c, \alpha_w)} (\Delta P + \Lambda)_x\end{aligned}\quad (3.7)$$

where

$$\begin{aligned}\tilde{\lambda}_c(\alpha_c, \alpha_w) &= \frac{\alpha_c^2 (\hat{\zeta}_w + \hat{\zeta}) + \alpha_w \alpha_c \hat{\zeta}}{[\hat{\zeta}_w \hat{\zeta}_c + \hat{\zeta} (\hat{\zeta}_w + \hat{\zeta}_c)]} \\ \tilde{\lambda}_T(\alpha_c, \alpha_w) &= \frac{\alpha_c^2 \hat{\zeta}_w + \alpha_w^2 \hat{\zeta}_c + (\alpha_c + \alpha_w)^2 \hat{\zeta}}{[\hat{\zeta}_w \hat{\zeta}_c + \hat{\zeta} (\hat{\zeta}_w + \hat{\zeta}_c)]}\end{aligned}\quad (3.8)$$

Equation (3.7) corresponds to the momentum equation in (3.1)₂ (ignoring the acceleration term and viscous term).

Next, let us see how we can identify an expression for the cell velocity u_c that explain the form of the cell mass balance (3.1)₁. We can eliminate the phase pressure gradient P_{wx} in (3.4) by multiplying by α_w and α_c in (3.4)₁ and (3.4)₂, respectively, and subtracting. Using that $u_w = \frac{U_T - \alpha_c u_c}{\alpha_w}$ this calculation

yields

$$\begin{aligned}
u_c &= \frac{\alpha_w \hat{\zeta} + \alpha_c (\hat{\zeta}_w + \hat{\zeta})}{\alpha_c^2 \hat{\zeta}_w + \alpha_w^2 \hat{\zeta}_c + (\alpha_c + \alpha_w)^2 \hat{\zeta}} U_T - \frac{\alpha_c \alpha_w^2}{\alpha_c^2 \hat{\zeta}_w + \alpha_w^2 \hat{\zeta}_c + (\alpha_c + \alpha_w)^2 \hat{\zeta}} (\Delta P + \Lambda)_x \\
&\approx \frac{\alpha_w \hat{\zeta} + \alpha_c \alpha_w (\hat{\zeta}_w + \hat{\zeta})}{\alpha_c^2 \hat{\zeta}_w + \alpha_w^2 \hat{\zeta}_c + (\alpha_c + \alpha_w)^2 \hat{\zeta}} u_w - \frac{\alpha_c \alpha_w^2}{\alpha_c^2 \hat{\zeta}_w + \alpha_w^2 \hat{\zeta}_c + (\alpha_c + \alpha_w)^2 \hat{\zeta}} (\Delta P + \Lambda)_x \\
&= \frac{\alpha_w \tilde{f}_c(\alpha_c, \alpha_w)}{\alpha_c} u_w - \frac{\tilde{h}(\alpha_c, \alpha_w)}{\alpha_c} \Delta P_x - \frac{\tilde{h}(\alpha_c, \alpha_w)}{\alpha_c} \Lambda_x \\
&:= u_{c1} + u_{c2} + u_{c3}
\end{aligned} \tag{3.9}$$

where cell migration u_c has three components: advective u_{c1} , diffusive u_{c2} and autologous chemotaxis u_{c3} ; and \tilde{f}_c and \tilde{h} take the form

$$\begin{aligned}
\tilde{f}_c(\alpha_c, \alpha_w) &= \frac{\alpha_c \alpha_w \hat{\zeta} + \alpha_c^2 (\hat{\zeta}_w + \hat{\zeta})}{\alpha_c^2 \hat{\zeta}_w + \alpha_w^2 \hat{\zeta}_c + (\alpha_c + \alpha_w)^2 \hat{\zeta}} \\
\tilde{h}(\alpha_c, \alpha_w) &= \frac{\alpha_c^2 \alpha_w^2}{\alpha_c^2 \hat{\zeta}_w + \alpha_w^2 \hat{\zeta}_c + (\alpha_c + \alpha_w)^2 \hat{\zeta}}
\end{aligned} \tag{3.10}$$

Remark 2. It should be noted that (3.10) is equivalent to (2.10) in light of (2.2)₁. Similarly for (3.8) versus (2.11) and (2.12). In the derivation of (3.8) and (3.10) we avoid using the relation (2.2)₁. This ensures that the discretization of the reduced model (3.1), which is presented in the next section, is consistent with the discretization of the more general biphasic model (2.6).

3.3. Numerical scheme implemented for the reduced model (3.1)

We assume that we have an approximate solution $(\alpha_{c,j}^k, C_j^k, P_{w,j}^k, u_{c,j+1/2}^k, u_{w,j+1/2}^k)$ at time t^k . Next, we describe how to obtain a new approximate solution $(\alpha_{c,j}^{k+1}, C_j^{k+1}, P_{w,j}^{k+1}, u_{c,j+1/2}^{k+1}, u_{w,j+1/2}^{k+1})$ at time t^{k+1} through a 3-step algorithm.

Step 1: Mass transport

We express the cell mass balance equation (3.1)₁ in terms of the cell velocity (3.9) and (3.10). Then we solve for $(\alpha_{c,j}^{k+1}, C_j^{k+1})$ by using the following discrete version of (3.1)₁ and (3.1)₃, respectively:

$$\frac{\alpha_{c,j}^{k+1} - \alpha_{c,j}^k}{\Delta t} + \frac{1}{\Delta x} ([\alpha_c u_c]_{j+1/2}^k - [\alpha_c u_c]_{j-1/2}^k) = 0 \tag{3.11}$$

where

$$[\alpha_c u_c]_{j+1/2}^k = \begin{cases} \alpha_{c,j}^k u_{c,j+1/2}^k, & \text{if } u_{c,j+1/2}^k \geq 0; \\ \alpha_{c,j+1}^k u_{c,j+1/2}^k, & \text{if } u_{c,j+1/2}^k < 0. \end{cases} \tag{3.12}$$

$$\frac{C_j^{k+1} - C_j^k}{\Delta t} + \frac{1}{\Delta x} ([C u_w]_{j+1/2}^k - [C u_w]_{j-1/2}^k) = \frac{D_c}{\Delta x} \left[\frac{C_{j+1}^k - C_j^k}{\Delta x} - \frac{C_j^k - C_{j-1}^k}{\Delta x} \right] + R_{C,j}^k \tag{3.13}$$

where

$$[C u_w]_{j+1/2}^k = \begin{cases} C_j^k u_{w,j+1/2}^k, & \text{if } u_{w,j+1/2}^k \geq 0; \\ C_{j+1}^k u_{w,j+1/2}^k, & \text{if } u_{w,j+1/2}^k < 0. \end{cases} \tag{3.14}$$

and

$$R_{C,j}^k = \lambda_1 \alpha_{c,j}^k (1 - \alpha_{c,j}^k) \left(1 - \left(\frac{C_j^k}{C_M}\right)^{v_2}\right) - (\lambda_2 \alpha_{c,j}^k + \lambda_3 T_{l,j}(P_{w,j}^k - \widetilde{P}_l^*)) C_j^k \quad (3.15)$$

Then, we compute $\alpha_{w,j}^{k+1}$ from (2.2)₁. Next, we compute pressure and fluid velocity simultaneously at time level $k + 1$.

Step 2: Computation of fluid velocity and pressure

We solve for $P_{w,j}^{k+1}$ and $u_{w,j+1/2}^{k+1}$ by considering the following algebraic system which is a discrete version of (3.1)₂:

$$\frac{1}{\Delta x} ([\alpha_w^{k+1} u_w^{k+1}]_{j+1/2} - [\alpha_w^{k+1} u_w^{k+1}]_{j-1/2}) = Q_j^{k+1} = T_{v,j}(\widetilde{P}_v^* - P_{w,j}^{k+1}) - T_{l,j}(P_{w,j}^{k+1} - \widetilde{P}_l^*) \quad (3.16)$$

which is combined with the momentum balance equation

$$\begin{aligned} & \rho \frac{u_{w,j+1/2}^{k+1} - u_{w,j+1/2}^k}{\Delta t} + \rho \frac{[u_w]_{j+1}^k \frac{u_{w,j+1/2}^{k+1} + u_{w,j+3/2}^{k+1}}{2}}{\Delta x} - \rho \frac{[u_w]_j^k \frac{u_{w,j-1/2}^{k+1} + u_{w,j+1/2}^{k+1}}{2}}{\Delta x} \\ & + \frac{1}{\Delta x} (P_{w,j+1}^{k+1} - P_{w,j}^{k+1}) = - \frac{\alpha_{w,j+1/2}^{k+1}}{\widetilde{\lambda}_T(\alpha_{c,j+1/2}^{k+1}, \alpha_{w,j+1/2}^{k+1})} u_{w,j+1/2}^{k+1} - \frac{\widetilde{\lambda}_c(\alpha_{c,j+1/2}^{k+1}, \alpha_{w,j+1/2}^{k+1})}{\widetilde{\lambda}_T(\alpha_{c,j+1/2}^{k+1}, \alpha_{w,j+1/2}^{k+1})} \cdot \frac{\Delta P(\alpha_{c,j+1}^{k+1}) - \Delta P(\alpha_{c,j}^{k+1})}{\Delta x} \\ & - \frac{\widetilde{\lambda}_c(\alpha_{c,j+1/2}^{k+1}, \alpha_{w,j+1/2}^{k+1})}{\widetilde{\lambda}_T(\alpha_{c,j+1/2}^{k+1}, \alpha_{w,j+1/2}^{k+1})} \cdot \frac{\Lambda(C_{j+1}^{k+1}) - \Lambda(C_j^{k+1})}{\Delta x} + \frac{\eta}{\Delta x^2} ([u_{w,j+3/2}^{k+1} - u_{w,j+1/2}^{k+1}] - [u_{w,j+1/2}^{k+1} - u_{w,j-1/2}^{k+1}]). \end{aligned} \quad (3.17)$$

where

$$[u_w]_{j+1}^k = \left[\frac{u_{w,j+1/2}^k + u_{w,j+3/2}^k}{2} \right] \quad (3.18)$$

for cell

$$[\alpha_c]_{j+1/2}^{k+1} = \begin{cases} \alpha_{c,j}^{k+1}, & \text{if } u_{c,j+1/2}^k - u_{w,j+1/2}^k > 0; \\ \frac{\alpha_{c,j+1}^{k+1} + \alpha_{c,j}^{k+1}}{2}, & \text{if } u_{c,j+1/2}^k - u_{w,j+1/2}^k = 0; \\ \alpha_{c,j+1}^{k+1}, & \text{if } u_{c,j+1/2}^k - u_{w,j+1/2}^k < 0. \end{cases} \quad (3.19)$$

for water

$$[\alpha_w]_{j+1/2}^{k+1} = \begin{cases} \alpha_{w,j}^{k+1}, & \text{if } u_{w,j+1/2}^k - u_{c,j+1/2}^k > 0; \\ \frac{\alpha_{w,j+1}^{k+1} + \alpha_{w,j}^{k+1}}{2}, & \text{if } u_{w,j+1/2}^k - u_{c,j+1/2}^k = 0; \\ \alpha_{w,j+1}^{k+1}, & \text{if } u_{w,j+1/2}^k - u_{c,j+1/2}^k < 0. \end{cases} \quad (3.20)$$

Step 3: Computation of cell velocity

After obtaining the water velocity $u_{w,j+1/2}^{k+1}$, the cell velocity is calculated based on (3.9) and (3.10).

$$u_{c,j+1/2}^{k+1} = \frac{\alpha_{w,j+1/2}^{k+1} \widetilde{f}_c(\alpha_{c,j+1/2}^{k+1}, \alpha_{w,j+1/2}^{k+1})}{\alpha_{c,j+1/2}^{k+1}} u_{w,j+1/2}^{k+1} - \frac{\widetilde{h}_c(\alpha_{c,j+1/2}^{k+1}, \alpha_{w,j+1/2}^{k+1})}{\alpha_{c,j+1/2}^{k+1}} \cdot \frac{\Delta P(\alpha_{c,j+1}^{k+1}) - \Delta P(\alpha_{c,j}^{k+1})}{\Delta x} - \frac{\widetilde{h}_c(\alpha_{c,j+1/2}^{k+1}, \alpha_{w,j+1/2}^{k+1})}{\alpha_{c,j+1/2}^{k+1}} \cdot \frac{\Lambda(C_{j+1}^{k+1}) - \Lambda(C_j^{k+1})}{\Delta x} \quad (3.21)$$

Herein, $\alpha_{c,j+1/2}^{k+1}$ and $\alpha_{w,j+1/2}^{k+1}$ appearing in (3.21) correspond to (3.19) and (3.20).

4. Results

A 1D spatial domain is considered with a realistic length 0.01m. We first present the numerical solution of the full two-phase cell-fluid-matrix model (2.6). A main purpose is to illustrate the ability of the model to create isolated groups of cancer cells as a result of proper tuning of the downstream and upstream mechanism. We also explore the role of parameters that characterize the cancer cell phenotype (i.e., strength of downstream versus upstream migration through $\hat{\zeta}$), as well as parameters that affect the fluid drainage through $T_v(x)$, $T_l(x)$, and internal vasculature pressure \widetilde{P}_l^* . Next, we compare the solution of the reduced model (3.1) with the same input data as the original model (2.6) where we also ignore the acceleration terms $\rho(\mathbf{u}_t + (\mathbf{u} \cdot \nabla)\mathbf{u})$ in the fluid momentum equation. For the cell-fluid regime we consider here, this part of the model plays a minor role. We also assess the possibility for further simplification of (3.1) by ignoring more terms in the fluid momentum equation (3.1)₂ as mentioned in Remark 1. Finally, we check how to accelerate the computations of the reduced model by reducing the number of updates of u_w and P_w in (3.1)₂.

For input data required to solve the model we refer to Table 1. The choice of these parameters are largely set as in [31] where the model was aligned to the experimental behavior as reported in [16]. We compute solutions after a time $T = 600$ (dimensionless) with reference time $T^* = 10^4 s$, which amounts to approximately 70 days.

Initial cell volume fraction and chemokine concentration

We consider an initial cell volume fraction (primary tumor) corresponding to

$$\alpha_c(x, t = 0) = 0.5 \exp(-[12.5(x - 0.5)]^2) \quad (4.1)$$

and initial chemokine is set to zero

$$C(x, t = 0) = 0. \quad (4.2)$$

Boundary conditions

The model is combined with the boundary conditions

$$P_w|_{\partial\Omega} = P^*, \quad \frac{\partial}{\partial \nu} C|_{\partial\Omega} = 0, \quad t > 0 \quad (4.3)$$

where ν is the outward normal on $\partial\Omega$ and $P^* = 0$ bar relatively the reference pressure 1 bar.

Table 1. Input parameters used in the full model (2.6) and reduced model (3.1).

Parameters	Description	Dimensional value
T^*	Reference time	10^4 s
L^*	Refence length	0.01 m
C^*	Reference chemokine density	10^{-4} kg/m ³
C_M	Maximal chemokine density	$0.3C^*$
D_C	Chemokine diffusion coefficient	5×10^{-13} m ² /s
Λ_1	Parameter characterizing Λ	40000 Pa
λ_1	Cell secretion rate	2.2×10^{-6} kg/(m ³ · s)
λ_2	Cell consumption rate	7.7×10^{-2} 1/s
λ_3	Absorption percentage	50%
ν_C	Related to logistic function	0.2
L	Domain length	0.01m
N	Number of grids	201
Δt	Time step interval	16s

Choice of input parameters

The following values are used for parameters related to the vascular flow, Q_v , given by (2.2)₄ and involved in the continuity equation for the fluid (2.6)₂:

$$T_v(x) = 5.6 \cdot 10^{-7} \text{ 1/(Pa} \cdot \text{s)}, \quad \tilde{P}_v^* = 5000 \text{ Pa} \approx 37.6 \text{ mmHg}, \quad x \in [0.4 \ 0.6] \quad (4.4)$$

and for lymphatic absorption Q_l in (2.2)₄ we use

$$T_l(x) = 5.6 \cdot 10^{-7} \text{ 1/(Pa} \cdot \text{s)}, \quad \tilde{P}_l^* = -700 \text{ Pa} \approx -5.3 \text{ mmHg} \quad x \in [0.25 \ 0.35] \cup [0.65 \ 0.75]. \quad (4.5)$$

Here the values of \tilde{P}_v^* and \tilde{P}_l^* are given relatively the reference pressure 1 bar (752 mmHg). Regarding $\Delta P(\alpha_c)$ given by (2.3), we set $\gamma = 1000$ Pa. For the various interaction forces $\hat{\zeta}_c$, $\hat{\zeta}_w$, and $\hat{\zeta}$ involved in (2.6)_{3,4} we use the following correlations [15, 26, 31]:

$$\hat{\zeta}_c = I_c \hat{k}_c \alpha_c^{r_c}, \quad \hat{\zeta}_w = I_w \hat{k}_w \alpha_w^{r_w}, \quad \hat{\zeta} = I \hat{k} \alpha_w \alpha_c^{1+r_{cw}}. \quad (4.6)$$

Parameters for the fluid-matrix interaction is set to

$$I_w = 2 \cdot 10^{12} \text{ Pa s/m}^2, \quad \hat{k}_w = 5, \quad r_w = 0 \quad (4.7)$$

and corresponding values for the cell-matrix interaction are set as

$$I_c = 200I_w, \quad \hat{k}_c = 1, \quad r_c = 0.5, \quad (4.8)$$

whereas the following set of parameters are used for the cell-fluid interaction term $\hat{\zeta}$:

$$I = -I_w, \quad \hat{k} = 4\hat{k}_w, \quad r_{cw} = 0.2. \quad (4.9)$$

The negative sign of I reflects a cell-generated mechanical force against the fluid flow direction. In Figure 1 we have plotted the fractional flow function $\hat{f}_c(\alpha_c)$ given by (3.10)₁ and coefficient function $\hat{h}(\alpha_c)$ given by (3.10)₂. Due to the negative coefficient I in the cell-fluid term $\hat{\zeta}$, the fractional flow function $\hat{f}_c(\alpha_c)$ contains a negative dip that gives rise to an upstream advective transport through u_{c1} , see (3.9) and (3.10). The upstream migration becomes larger with larger values of u_w and increases with higher volume fraction of cells.

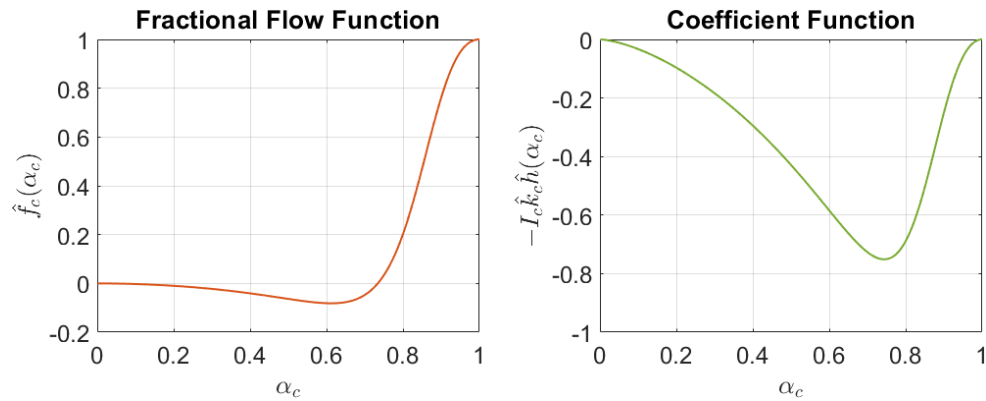


Figure 1. An illustration of $\hat{f}_c(\alpha_c)$ (left) and $-I_c\hat{k}_c\hat{h}(\alpha_c)$ (right) defined by (2.10).

4.1. The cell-fluid-matrix model (2.6)

We first illustrate a cell progression pattern after a time $T = 600$ by using the model (2.6) and the corresponding numerical scheme described in Section 2.3. Figure 2(A) shows the relevant position of the leaky intratumoral vasculature (through T_v) and collecting peritumoral lymphatic vessels (through T_l). As seen from Figure 2(A), lymphatic vessels are essentially non-functional in the initial cell region and the fluid is forced to flow towards the peritumoral region, which can be seen from the velocity u_w profile in Figure 2(D). Note that the positive value of velocity u_w represents flow from left to right in the domain, vice versa. This outward flow of fluid gives rise to the fluid pressure P_w (blue) shown in Figure 2(F). Chemokine C is secreted by the cancer cells and goes with the fluid flow towards the lymphatic region where it tends to accumulate and create higher concentrations, see panel (C). This triggers a chemotactic-driven outgoing cell migration. At the same time, the strong fluid velocity found at the tumor periphery generates a relatively strong mechanical-driven upstream migration. What is interesting is that the cells' upstream migration due to fluid flow is almost offset by the velocity components due to diffusion and chemotaxis in the middle region of domain where there seems to be close to zero total velocity, see Figure 2(E). However, the velocity caused by chemotaxis dominates the total cell velocity in the region outside the primary tumor where the upstream migration effect is relatively low due to the low cell volume fraction, thus leading to detachment of cancer cells on both sides of the primary tumor, see Figure 2(B). The net effect is, as seen from panel (B), that the primary tumor is largely kept intact while islands of cancer cells are formed in the peritumoral region. This demonstrates how the experimentally observed migration mechanisms reported in [16,17,24] may serve as an effective means for lymph node metastases.

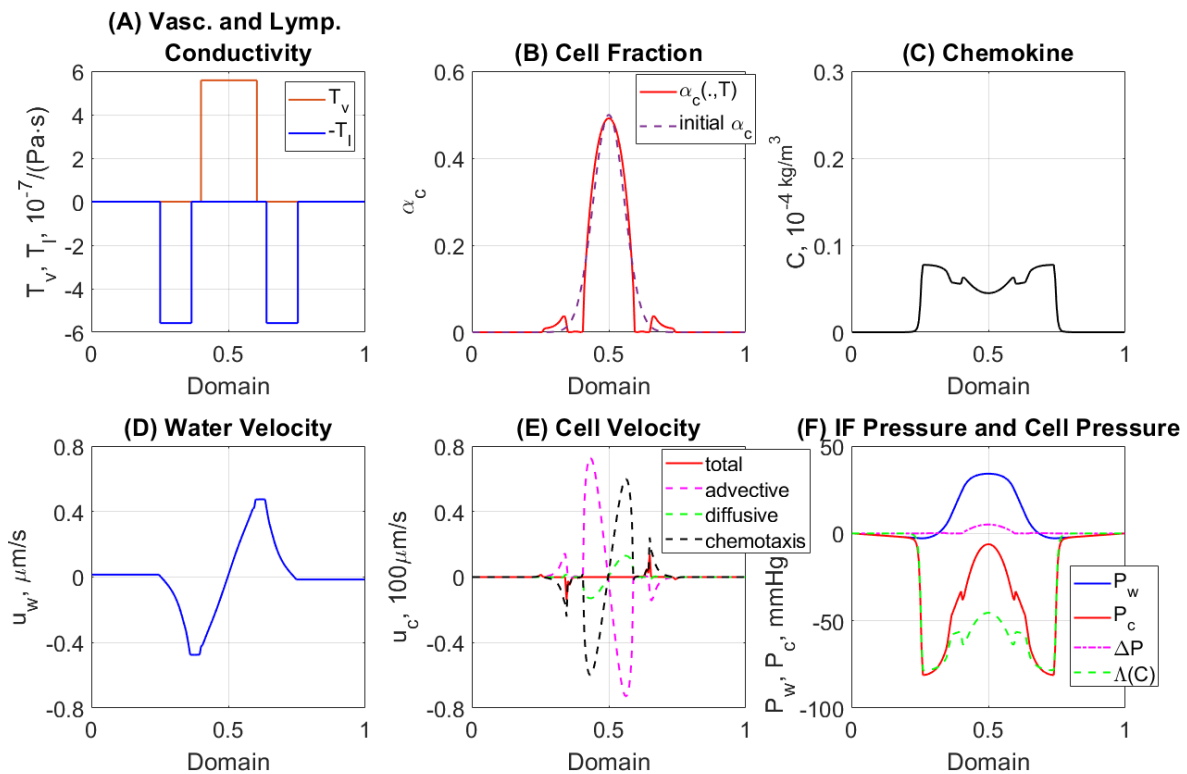


Figure 2. Results using the full model (2.6) at $T=600$. Two isolated islands of detached cells are formed near the main cell region. (A) Vasculature conductivity T_v and lymphatic conductivity T_l . (B) Cell volume fraction α_c . (C) Chemokine concentration C . (D) Fluid velocity u_w . (E) Cell velocity u_c . (F) Fluid pressure P_w , cell pressure P_c together with capillary pressure ΔP and chemotaxis potential Λ .

What is the role of the upstream migration for generating cancer cell detachment

In this example, we modify the cell-fluid interaction term in (4.9) and reduce the upstream effect by a factor 2 by setting $\hat{k} = 2\hat{k}_w$. Figure 3 illustrates the corresponding result. In panel (B) we see that most of the cells move towards the lymphatic region since the upstream velocity component is reduced. Most strikingly, there is no detachment mechanism that can create cell islands, as shown in Figure 2(B). The chemokine concentration profile in panel (C) is quite smooth due to a higher consumption rate with higher cell volume fraction. As a consequence, as seen in panel (E), both the upstream component and the chemotactic component of cell velocity are rather small compared to the case in Figure 2(E). This shows how the upstream migration of cells caused by fluid flow plays a vital role in forming detached islands of cells.

What is the effect of the vasculature and lymphatic conductivities T_v and T_l

In this example, we use a heterogeneous distribution of the vasculature and lymphatic conductivities T_v and T_l , see panel (A) in Figure 4, rather than a constant value as in the example in Figure 2(A). A first observation from Figure 4(B) is that a new isolated island is formed on each side of the primary tumor, in addition to the old one shown in Figure 2(B). This is consistent with the non-uniform distribution of the lymphatic vessels through T_l shown in Figure 4(A). Looking at the cell velocity components

in Figure 4(E), it is clear that the upstream mechanical-driven cell velocity (pink) and downstream chemical-driven (black) have opposite sign. The detachment mechanism observed for the base case (in Figure 2) is at work again and is able to generate a second island, by the help of the non-uniform absorption of fluid described through T_l . The heterogeneous lymphatic vessels influence the source term in the chemokine equation (2.20) and fluid velocity (Figure 4(D)) through the mass transport equation (2.21).

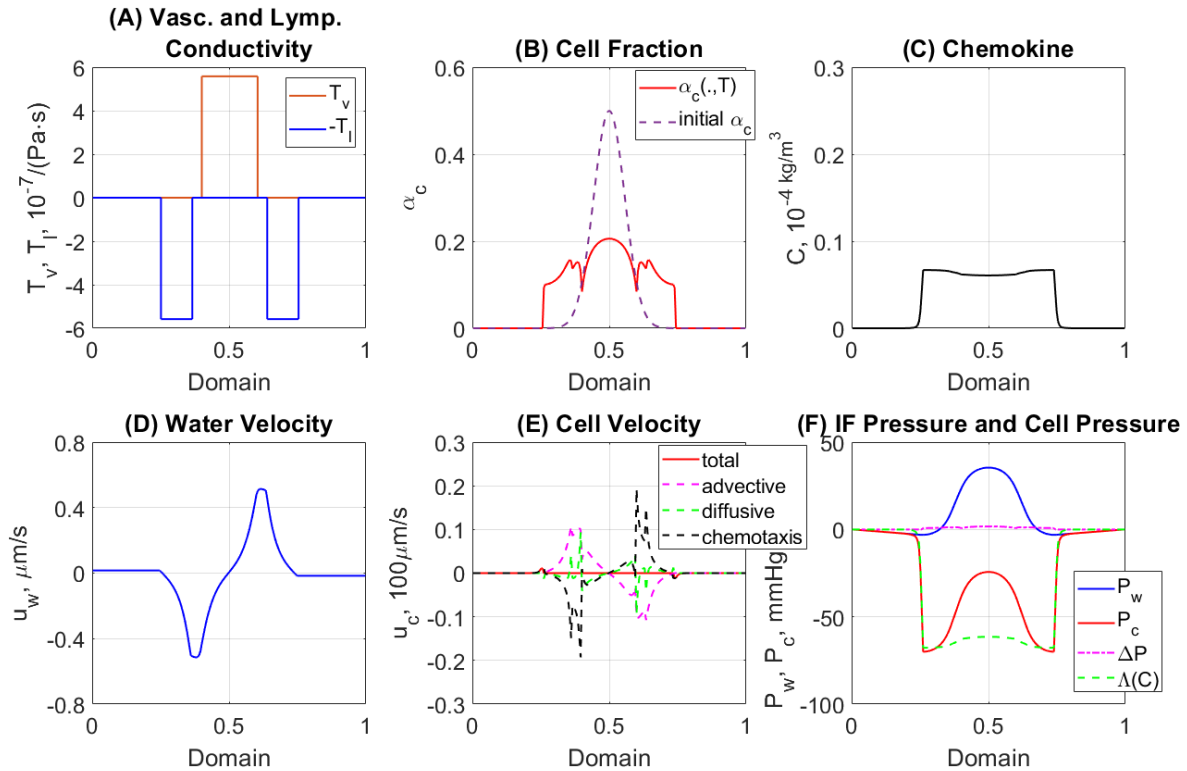


Figure 3. Results using the full model (2.6) at $T=600$. We reduce the upstream effect of cell migration by setting $\hat{k} = 2\hat{k}_w$ in (4.9). The results show that a large portion of the cells move towards the lymphatic region, however, there is no formation of islands in this case. Subplots are explained in Figure 2.

*What is the role of the internal lymphatic vasculature pressure \tilde{P}_l^**

The role of lymph nodes for cancer cell migration to and through lymphatic vessels, survival in draining lymph nodes and further spread to other distant organs, is currently intensely debated [11, 32, 38]. In Figure 5 we run the base again but the value of the internal lymphatic vasculature pressure \tilde{P}_l^* in (4.5) take two different values: for the left region $\tilde{P}_l^* = -7.5$ mmHg and for the right region $\tilde{P}_l^* = -3$ mmHg. As we can expect, the fluid pressure P_w in Figure 5(F) takes a lower value in the left region (i.e., a stronger absorption of fluid) compared to the right side. Moreover, the maximal water velocity u_w in the right domain is lower than the one in the left side. This affects the distribution of chemokine C within the fluid phase seen in panel (C). As a result, the cell velocity component due to chemotaxis seen in Figure 5(E) is smaller in the peritumoral region on the right side. In turn, the developed isolated island of cells on the right side of the primary tumor becomes smaller, as compared to the left hand side island.

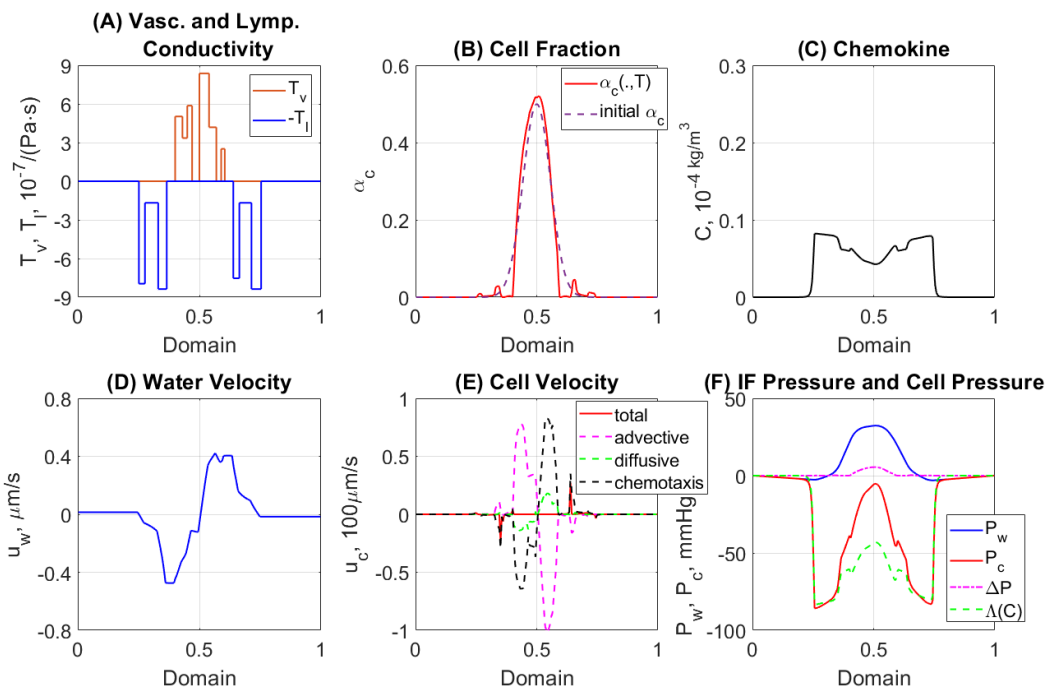


Figure 4. Results using the full model (2.6) at $T=600$. We use random distribution of T_v and T_l (panel A) in $(2.2)_5$. The heterogeneity of lymphatic conductivities generates more islands compared to Figure 2. Subplots are explained in Figure 2.

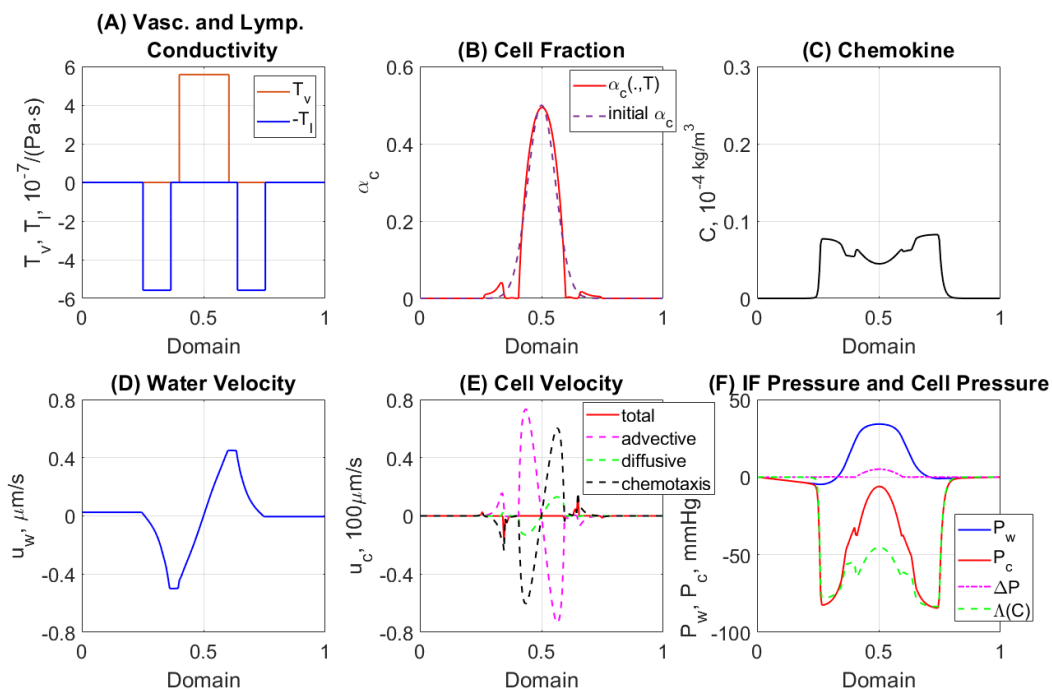


Figure 5. Results using the full model (2.6) at $T=600$. We use $\tilde{P}_i^*(0.25 < x < 0.35) = -7.5 \text{ mmHg}$ and $\tilde{P}_i^*(0.65 < x < 0.75) = -3 \text{ mmHg}$ in $(2.2)_5$. Subplots are explained in Figure 2.

4.2. The reduced cell-fluid-matrix model (3.1)

Now our question is: can we use the reduced cell-fluid model (3.1) to reproduce the same behavior as seen for the full model in Figure 2? The potential benefits of this investigation is that it can not only help us to speed up our simulations, especially when there is a need for huge amounts of output data, but it can also provide further insight into the cell-fluid migration mechanisms. We use the same input data as the base case in Figure 2 and make use of the reduced model (3.1) with its corresponding numerical scheme developed in Sec.3.3. Figure 6 shows the result for the reduced model and the plots are compared with those from the full two-fluid model (2.6). Clearly, a nice match is seen between the reduced model and the full model. This verifies that the key elements of the migration mechanisms are kept in the reduced model.

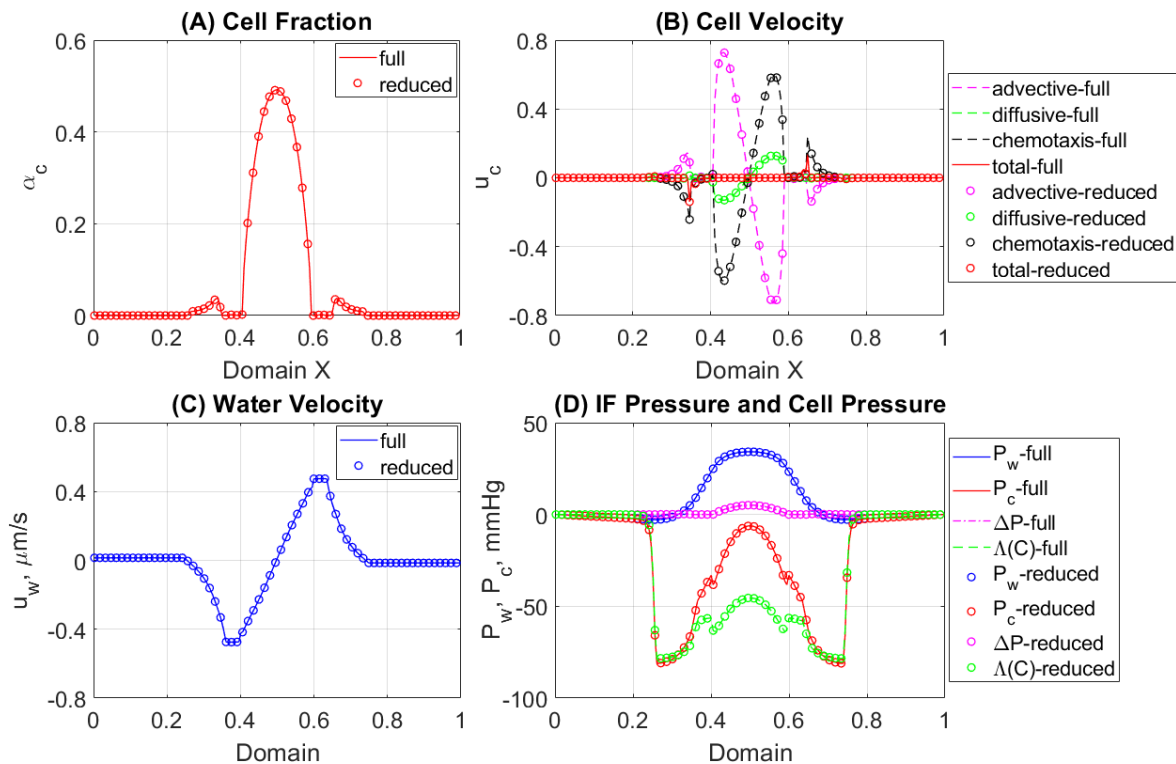


Figure 6. Results using the reduced model (3.1) compared with those from the full two-fluid model (2.6) at $T=600$. We use the same input data as the base case in Figure 2. The results are practically speaking the same for the reduced model and the full model. Subplots are explained in Figure 2.

Features of the reduced model (3.1)

In view of the above comparison of the reduced model (3.1) and the original (2.6) two natural questions are: (i) Can we take a step further in decoupling the fluid flow dynamics and cell migration dynamics by ignoring the extra pressure terms $\frac{\lambda_c}{\lambda_r} \nabla(\Delta P(\alpha_c) + \Lambda(C))$ in the momentum equation in (3.1)₂, as commented in Remark 1? (ii) Is it possible to speed up the computation efficiency of the reduced model? To answer the first question, we run the reduced model where we have ignored this term, i.e., setting ΔP and Λ as 0. A comparison is shown in Figure 7(A1, B1). Clearly, the results are

quite similar. The reason can be explained by the fact that the coefficient ($\frac{\lambda_c}{\lambda_T}$, cell fraction flow) takes a rather small value due to the low mobility of cancer cells. Consequently, for the current fluid-cell-matrix “flow regime” it makes perfect sense to remove the impact from cancer cells on the fluid through these pressure-related terms. It might be tempting to suggest a further decoupling between fluid and cells by replacing $\nabla \cdot (\alpha_w \mathbf{u}) = Q$ by $\nabla \cdot \mathbf{u} = Q$ as indicated in Remark 1. Numerical investigations indicate that this completely changes the tumor progression behavior. This is quite reasonable since the volume fraction of cancer cells α_c typically can be relatively high at the tumor periphery where the fluid velocity u_w is strongest, and the presence of cancer cell phase cannot be ignored.

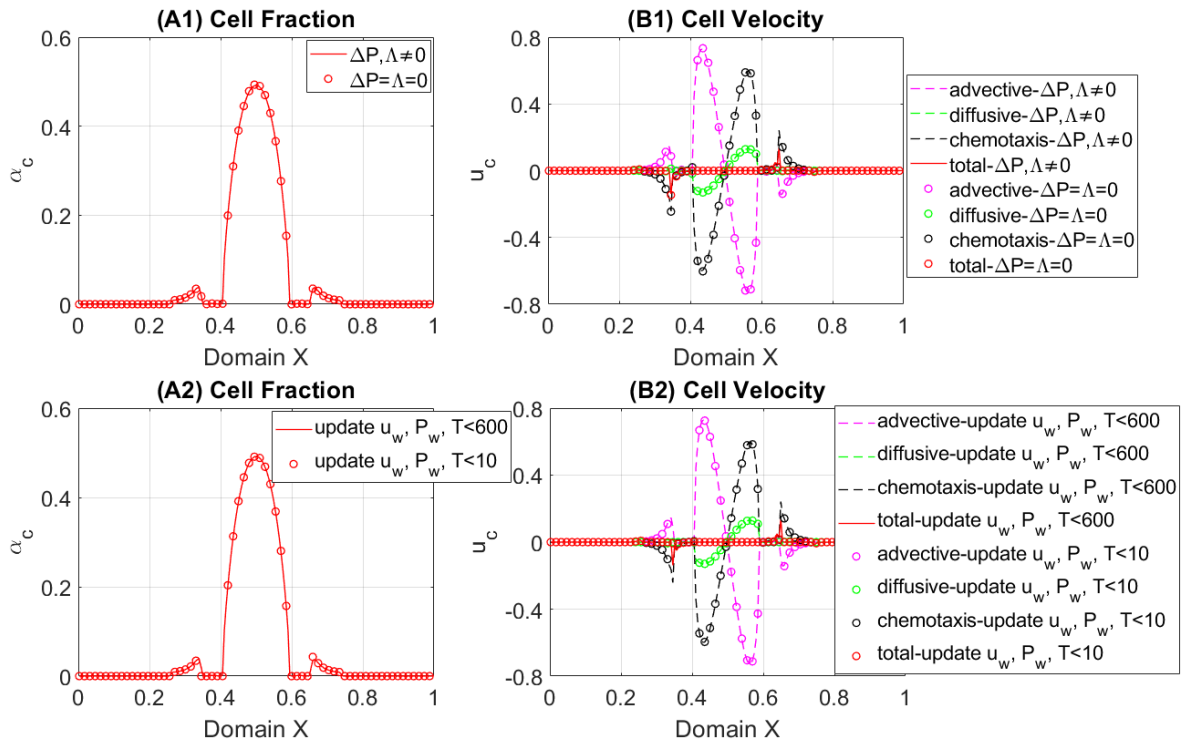


Figure 7. Results using the reduced model (3.1) at $T=600$. (A1,B1): *Solid line* - include ΔP and Λ in the momentum equation (3.1)₂. *Bullet points* - ignore ΔP and Λ in the momentum equation (3.1)₂. (A2, B2): *Solid line* - numerical algorithm in Sec. 3.3 with full coupling between Steps (1–3) through the time period $[0, 600]$. *Bullet points* - numerical algorithm in Sec. 3.3 where we only use full coupling between Steps (1–3) through the time period $[0, 10]$ with no further updates of u_w and P_w (step 2) for $t > 10$.

Finally, what about point (ii)? We want to check the possibility of accelerating the computations of the reduced model by decreasing the number of updates of u_w and P_w in Step 2 (Section 3.3) of the numerical algorithm. Based on our tests, we find that at the early stage of the simulation, the cell-fluid dynamics is quite fast. So, at that stage it is necessary with a tight coupling, as described by the algorithm in Section 3.3. However, after a time $t = 10$, when the fluid and pressure field have been established, we stop updating u_w and P_w . The result of this is shown in Figure 7(A2, B2). Clearly, it works perfectly well to strongly reduce the updates of u_w and P_w (after an initial transient time period till $t = 10$). We can see hardly no difference between this simplified calculation of u_w and P_w and the scheme where u_w and P_w are updated for every Δt .

5. Concluding remarks

The main findings from our investigations in a one-dimensional tumor setting are:

- (i) We have verified that a novel discretization of the general biphasic cell-fluid-matrix model (2.6) reliably can deal with the competing migration mechanisms, one that triggers downstream chemotactic migration, another which gives rise to a mechanical driven upstream. In particular, we find that these two opposite migration mechanisms, when properly tuned, do not cancel out each other but instead can be a means to form isolated groups of cancer cells that are situated in the region outside the primary tumor and close to lymphatic vessels. This detachment mechanism reflects an aggressive behavior that might be linked to lymph node metastases where cancer cells are able to escape through lymphatic vessels [4, 11, 38].
- (ii) The cancer cells are responsible for formation of a leaky and aberrant intratumoral vasculature modeled through the source term Q_v as well as remodelling of the matrix structure and density, which affect the tissue conductivity as represented through the fluid-matrix resistance force coefficient $\hat{\zeta}_w$. Hence, implicitly the cancer cells affect the fluid velocity field \mathbf{u}_w and fluid pressure P_w , as expressed by the pressure equation (2.14). Here we note that total mobility $\hat{\lambda}_T$ (2.12) is dominated by fluid mobility $\hat{\lambda}_w$ in the presence of both phases since from (2.11) it follows that $\frac{\lambda_c}{\lambda_w} \sim \frac{\alpha_c^2 \hat{\zeta}_w}{\alpha_w^2 \hat{\zeta}_c} \sim \frac{l_w}{l_c} \sim 0.005$ in view of (4.8). In the current version of the model the vasculature and tissue conductivity through Q_v and $\hat{\zeta}_w$ are assumed to be stationary. By taking advantage of the fact that explicit presence of cancer cells in the model (2.6) has a weaker impact on the fluid, we have identified a chemotaxis-Navier-Stokes version (3.1) which bears similarity to the much studied cell-fluid model for cell swimming (3.3) [29]. It has been verified that the behavior of the full model (2.6) largely carries over to the reduced model (3.1).
- (iii) As a byproduct we have found that the numerical discretization we employ can be greatly accelerated by taking advantage of the fact that the fluid pressure and velocity possibly change slowly as compared to the cell migration.

What is the potential importance of the findings presented in this work? The usefulness of the proposed numerical scheme for (2.6) and (3.1) lies in the the fact that it can naturally be extended to include compressible phases and viscous terms as well as more cell types that also are involved. For example, other cells like stromal cells and immune cells play important roles, depending on the special application of the model. In order to use the model for a more real-life situation where one has access to data through MRI images, etc, it will necessary to study the model in 2D and 3D setting. Methods used to relate the model to available data require many simulations. Hence, the possibility to accelerate computations is essential. The reduced model and its discrete counterpart opens for such applications. Combination with novel machine learning based frameworks [14] can potentially lead to even more efficient calculations.

Lymph node metastasis is a main reason why cancer becomes a deadly disease [11]. That is, instead of just having a growing coherent tumor, the tumor evolves into a heterogeneous mix of aggressive cancer cell phenotypes that can make use of different migration mechanisms for detachment. The model we explore contains a specific mechanism for creating isolated groups of cancer cells that are located in the peritumoral region. A natural question to raise in this context is: What are critical parameters that determine the relative strength of the various migration mechanisms

involved in the model (2.6) and its simplified version (3.1)? As explored in Section 4, whether the model gives rise to aggressive behavior or not depends on a fine-tuned balance between the magnitude of different forces that are involved, as expressed through the momentum balance equations. Mathematical analysis can detect finer details pertaining to such issues, insight that may not easily be detected from numerical simulations. Long time behavior and asymptotic behavior represents particular areas of interest. Singular behavior (in a broad sense), e.g., formation of isolated islands that are able to persist over long time, are of interest. A simplified version of a model similar to (2.5) has been investigated in a one-dimensional setting in [9]. Similarly, the competing downstream and upstream migration were explored by mathematical methods in [10] and precise statements of the long-time behavior were detected under appropriate constraints. An interesting question is whether such results can be taken over to more general models as discussed in this manuscript.

The chemotaxis-Navier-Stokes model (3.3) has attracted extensive interest the last two decades. A main question is to what extent various results known to hold for a pure chemotaxis model still hold under the influence of a fluid velocity field described by the (Navier-)Stokes model [34] influenced by the cell population through buoyancy. This include results on global solvability and blow-up behavior (critical parameters), e.g., [1, 3, 6, 13, 27, 28, 35, 36] and references therein, as well as long-time behavior [33]. An interesting question is whether the model includes the possibility to represent spatial-dependent patterns over long time [29]. The long-time result in [33] ensures in a precise sense that the cell population will converge to a constant state without spatial variations. In the context of the tumor model, this amounts to a situation where isolated groups of cancer cells cannot persist over time. In that light an interesting question is whether it is possible to build on the experience with the analysis of the Tuval model to obtain qualitative insight into the solutions generated by the tumor model (3.1) or an appropriate modification/simplification of it.

Acknowledgments

The first author thanks the University of Stavanger for funding of the postdoc position.

Conflict of interest

The authors declare no conflict of interest.

References

1. T. Black, Global very weak solutions to a chemotaxis-fluid system with nonlinear diffusion, *SIAM J. Math. Anal.*, **50** (2018), 4087–4116.
2. H. M. Byrne, M. R. Owen, A new interpretation of the Keller-Segel model based on multiphase modelling, *J. Math. Biol.*, **49** (2004), 604–626.
3. X. Cao, Fluid interaction does not affect the critical exponent in a three-dimensional Keller-Segel-Stokes model, *Z. Angew. Math. Phys.*, **71** (2020), 61.
4. A. Chhetri, J. V. Rispoli, S. A. Lelievre, 3D cell culture for the study of microenvironment-mediated mechanostimuli to the cell nucleus: An important step for cancer research, *Front. Mol. Biosci.*, **8** (2021), 628386.

5. D. A. Drew, S. L. Passman, *Theory of multicomponent fluids*, Springer, 1999.
6. M. Di Francesco, A. Lorz, P. Markowich, Chemotaxis-fluid coupled model for swimming bacteria with nonlinear diffusion: global existence and asymptotic behavior, *DCDS*, **28** (2010) 1437–1453.
7. S. Evje, An integrative multiphase model for cancer cell migration under influence of physical cues from the microenvironment, *Chem. Eng. Sci.*, **165** (2017), 240–259.
8. S. Evje, J. O. Waldeland, How tumor cells can make use of interstitial fluid flow in a strategy for metastasis, *Cell. Mol. Bioeng.*, **12** (2019), 227–254.
9. S. Evje, H. Wen, A Stokes two-fluid model for cell migration that can account for physical cues in the microenvironment, *SIAM J. Math. Anal.*, **50** (2018), 86–118.
10. S. Evje, M. Winkler, Mathematical analysis of two competing cancer cell migration mechanisms driven by interstitial fluid flow, *J. Nonlinear Sci.*, **30** (2020), 1809–1847.
11. G. Follain, D. Herrmann, S. Harlepp, V. Hyenne, N. Osmani, S. C. Warren, et al., Fluids and their mechanics in tumour transit: shaping metastasis, *Nat. Rev. Cancer*, **20** (2020), 107–124.
12. U. Haessler, J. C. M. Teo, D. Foretay, P. Renaud, M. A. Swartz, Migration dynamics of breast cancer cells in a tunable 3D interstitial flow chamber, *Integr. Biol.*, **4** (2012), 401–409.
13. A. Lorz, Coupled Keller-Segel-Stokes model: global existence for small initial data and blow-up delay, *Commun. Math. Sci.*, **10** (2012), 555–574.
14. S. Mishra, A machine learning framework for data driven acceleration of computations of differential equations, *Math. Eng.*, **1** (2019), 118–146.
15. J. A. Pedersen, S. Lichter, M. A. Swartz, Cells in 3D matrices under interstitial flow: effects of extracellular matrix alignment on cell shear stress and drag forces, *J. Biomech.*, **43** (2010), 900–905.
16. W. J. Polacheck, J. L. Charest, R. D. Kamm, Interstitial flow influences direction of tumor cell migration through competing mechanisms, *Proc. Natl. Acad. Sci. U.S.A.*, **108** (2011), 11115–11120.
17. W. J. Polacheck, A. E. German, A. Mammoto, D. E. Ingber, R. D. Kamm, Mechanotransduction of fluid stresses governs 3D cell migration, *Proc. Natl. Acad. Sci. U.S.A.*, **111** (2014), 2447–2452.
18. Y. Qiao, P. Ø. Andersen, S. Evje, D. C. Standnes, A mixture theory approach to model co-and counter-current two-phase flow in porous media accounting for viscous coupling, *Adv. Water Resour.*, **112** (2018), 170–188.
19. Y. Qiao, S. Evje, A general cell–fluid Navier-Stokes model with inclusion of chemotaxis, *Math. Models Methods Appl. Sci.*, **30** (2020), 1167–1215.
20. Y. Qiao, S. Evje, A compressible viscous three-phase model for porous media flow based on the theory of mixtures, *Adv. Water Resour.*, **141** (2020), 103599.
21. Y. Qiao, H. Wen, S. Evje, Viscous two-phase flow in porous media driven by source terms: analysis and numerics, *SIAM J. Math. Anal.*, **51** (2019), 5103–5140.
22. K. R. Rajagopal, On a hierarchy of approximate models for flows of incompressible fluids through porous solids, *Math. Models Methods Appl. Sci.*, **17** (2007), 215–252.

23. G. S. Rosalem, E. B. L. Casas, T. P. Lima, L. A. Gonzalez-Torres, A mechanobiological model to study upstream cell migration guided by tensotaxis, *Biomech. Mod. Mech.*, **19** (2020), 1537–1549.
24. J. D. Shields, M. E. Fleury, C. Yong, A. A. Tomei, G. J. Randolph, M. A. Swartz, Autologous chemotaxis as a mechanism of tumor cell homing to lymphatics via interstitial flow and autocrine CCR7 signaling, *Cancer Cell*, **11** (2007), 526–538.
25. D. C. Standnes, S. Evje, P. Ø. Andersen, A novel relative permeability model based on mixture theory approach accounting for solid–fluid and fluid–fluid interactions, *Tran. Por. Med.*, **119** (2017), 707–738.
26. M. A. Swartz, M. E. Fleury, Interstitial flow and its effects in soft tissues, *Annu. Rev. Biomed. Eng.*, **9** (2007), 229–256.
27. Y. Tao, M. Winkler, Global existence and boundedness in a Keller-Segel-Stokes model with arbitrary porous medium diffusion, *DCDS*, **32** (2012), 1901–1914.
28. Y. Tao, M. Winkler, Locally bounded global solutions in a three-dimensional chemotaxis-Stokes system with nonlinear diffusion, *Ann. Inst. H. Poincaré Anal. Non Linéaire*, **30** (2013), 157–178.
29. I. Tuval, L. Cisneros, C. Dombrowski, C. W. Wolgemuth, J. O. Kessler, R. E. Goldstein, Bacterial swimming and oxygen transport near contact lines, *Proc. Natl. Acad. Sci. U.S.A.*, **102** (2005), 2277–2282.
30. J. O. Waldeland, S. Evje, A multiphase model for exploring cancer cell migration driven by autologous chemotaxis, *Chem. Eng. Sci.*, **191** (2018), 268–287.
31. J. O. Waldeland, S. Evje, Competing tumor cell migration mechanisms caused by interstitial fluid flow, *J. Biomech.*, **81** (2018), 22–35.
32. H. Wiig, M. A. Swartz, Interstitial fluid and lymph formation and transport: physiological regulation and roles in inflammation and cancer, *Physiol Rev.*, **92** (2012), 1005–1060.
33. M. Winkler, Stabilization in a two-dimensional chemotaxis-Navier-Stokes system, *Arch. Rational Mech. Anal.*, **211** (2014), 455–487.
34. M. Winkler, Does fluid interaction affect regularity in the three-dimensional Keller-Segel system with saturated sensitivity?, *J. Math. Fluid Mech.*, **20** (2018), 1889–1909.
35. M. Winkler, Small-mass solutions in the two-dimensional Keller-Segel system coupled to the Navier–Stokes equations, *SIAM J. Math. Anal.*, **52** (2020), 2041–2080.
36. M. Winkler, Global weak solutions in a three-dimensional Keller-Segel-Navier-Stokes system with gradient-dependent flux limitation, *Nonlinear Anal. Real*, **59** (2021), 103257.
37. Y. S. Wu, *Multiphase fluid flow in porous and fractured reservoirs*, Elsevier, 2016.
38. H. Zhou, P. Lei, T. P. Padera, Progression of metastasis through lymphatic system, *Cells*, **10** (2021), 627.



AIMS Press

©2022 the Author(s), licensee AIMS Press. This is an open access article distributed under the terms of the Creative Commons Attribution License (<http://creativecommons.org/licenses/by/4.0>)